



Tyramine Adsorption Using the Modification of Takari Natural Sand-Based Silica with Bovine Serum Albumin (BSA)

Johnson N. Naat^{1*}, Yantus A. B Neolaka¹, Yosep Lawa¹, Petrus M. Noning¹, Ayu W. M. Menno¹, Rosnita¹, Fransiskus B.O. Weo¹, Dewi Lestarani¹, Sri Sugiarti², Dyah Iswanti^{2*}

¹University of Nusa Cendana, Kupang, Chemistry Education Department, Faculty of Education and Teachers Training, East Nusa Tenggara, 85001, Indonesia

²Bogor Agricultural University, Department of Chemistry, Bogor, 16144, Indonesia

Abstract: In this article, we use a batch method to convey tyramine adsorption by modifying Takari natural sand-based silica with BSA and tyramine adsorption. The research stages include the optimization of adsorbent mass, pH, temperature, determination of the isotherm model, and thermodynamic parameters of tyramine adsorption. The tyramine concentration was determined using UV-Vis. The characterizations carried out were functional groups using FT-IR and surface morphology using SEM. The results of FT-IR characterization demonstrated the success of BSA modification, as observed in the C-H, N-H, and C-N groups, which are the typical functional groups of BSA. The SEM image of SiO₂@BSA before tyramine adsorption revealed unevenly sized particles, uneven distribution, and agglomeration, leading to larger particles. The morphology of SiO₂@BSA-tyramine appeared to be more uniform, exhibiting a smoother shape with a slightly uneven surface. The optimum pH was 5 ($q_e=11.74$ mg/g), and the optimum temperature was 303 K ($q_e= 2.47$ mg/g). The isotherm study showed that the adsorption adhered to the Redlich-Peterson isotherm model with an R^2 value of 0.987 ($q_e=5.157$ mg/g and $n =3.759$). The thermodynamic study demonstrated $\Delta H^\circ = 49.08$ kJ/mol, $\Delta G^\circ = -17.84; -20.05$ and -22.26 kJ/mol, and $\Delta S^\circ = 0.22$ kJ/mol.K. These results indicated that the tyramine adsorption process on SiO₂@BSA adsorbent occurred endothermically and spontaneously at the temperature of 303 K, and the adsorption was of a physical-chemical adsorption type.

Keywords: Takari natural sand, adsorption, SiO₂@BSA, kinetics, isotherm, thermodynamics, tyramine.

Submitted: January 31, 2023. **Accepted:** July 10, 2023.

Cite this: Naat JN, Neolaka YA, Lawa Y, Noning PM, Menno AWM, Rosnita, Weo FBOW, Lestarani D, Sugiarti S, Iswanti D. Tyramine Adsorption Using the Modification of Takari Natural Sand-Based Silica with Bovine Serum Albumin (BSA). JOTCSA. 2023;10(4):929-40.

DOI: <https://doi.org/10.18596/jotcsa.1244774>.

***Corresponding author.** E-mail: johnson_naat@staf.undana.ac.id; dyahprado@yahoo.co.id

1. INTRODUCTION

Tyramine is one of the biogenic amine compounds formed from the amino acid tyrosine through a decarboxylation process with the help of the aromatic amino acid decarboxylase enzyme (1). Tyramine can be found in several types of food and beverages, including cheese, fish, fresh meat, fermented meat and vegetables, tomatoes, bananas, prunes, and alcoholic beverages (2-4). Tyramine is essential in the human body in controlling blood pressure by raising blood pressure (3). However, consuming foods or

beverages containing high tyramine can cause adverse effects, namely causing high blood pressure (3, 4), gastric acid hypersecretion, migraine, increased blood sugar levels (5, 6), and toxicity. Higher than histamine, which can cause cell death (7). Therefore, it is necessary to overcome the adverse effects of tyramine. Standard methods used for the determination of tyramine include the extraction and purification of the analyte using acidic solvents such as hydrochloric acid or trichloroacetic acid (8), high-performance liquid chromatography (HPLC) (9), capillary electrophoresis (CE) (10), and thin-layer

chromatography/densitometry (TLC) (11). While these methods are effective, they require expensive equipment, reagent preparation and can be challenging to operate. One method that has been carried out is the adsorption method (12–14). The adsorption method's advantages include using low-cost reagents, simple operation, rapid action, high efficiency, and low cost (15). Adsorption is a mass transfer event on the surface of the adsorbent particles (16). Adsorption occurs because of the attractive force between the adsorbate molecules and the molecules or atoms that compose the surface of the adsorbent (17). The use of the adsorption method as a solution to reduce and remove tyramine has been carried out with several adsorbents, including carbon nanotubes (13), zirconium phosphate (18), Ca-montmorillonite (14), and silica (12).

Silica has an active site in the form of a silanol group ($\equiv\text{SiOH}$) and a siloxane group ($\equiv\text{Si-O-Si}\equiv$) on its surface, thus having polar and hydrophilic qualities (17, 19). Many uses of silica as an adsorbent are based on silica's advantages, which are stable in acidic conditions, not expandable, and high-temperatures resistant. Silica also has a high-mass exchange, good porosity, and a large surface area (19, 10). However, silica has the disadvantage of low surface selectivity and effectiveness. This is because the active sites of silica only have silanol and siloxane groups in which the silanol group consists of oxygen which has a weak ability as an electron pair donor (19–21). To overcome this weakness, the silica surface can be modified by adding organic functional groups to the silica surface (22). One of the ways is to use bovine serum albumin (BSA) (12).

BSA is a protein transporting various chemical compounds in bovine blood (12). The advantages of BSA as a modifying agent are biocompatibility, biodegradability, up to 60 °C for approximately 10 hours of heat resistance, stability at pH 4-9, and non-toxic. BSA also has high solubility at pH 7.4 and good ligand connection properties (23-25). These advantages make BSA a safe modifier of silica modification for tyramine adsorption.

The factors of mass, pH, temperature, and concentration influence the effectiveness of adsorption. Adsorption capacity by $\text{SiO}_2\text{@BSA}$ adsorbent can vary depending on the mass composition and pH of the solution to determine the interaction of adsorbent and adsorbate (14). Adsorption isotherm studies were conducted to obtain information about the phenomena and interactions between adsorbate and adsorbent. Several adsorption isotherm models of tyramine can predict adsorption performance because adsorption isotherm models can provide information about adsorbent capacity, adsorption mechanism, and evaluation of adsorption process performance (26). In addition, the temperature of the solution affects the adsorbent's ability to adsorb, and thermodynamic studies determine what kind of adsorption process takes place.

Adsorption can exhibit spontaneous or non-spontaneous behavior and can be characterized as exothermic or endothermic. The adsorption properties can be physical, chemical, or a combination of both (27). Previous studies have not widely reported research and reports related to the adsorption and degradation of tyramine, so it is a novelty in this reported article. This article conveys the mass, optimum pH, temperature, eight isotherm models, and thermodynamic parameters of tyramine adsorption using the modification of Takari natural sand-based silica with BSA.

2. EXPERIMENTAL SECTION

2.1. Materials

Takari natural sand, histamine hydrochloride ($\text{C}_8\text{H}_{11}\text{NO}\cdot\text{HCl}$), Bovine Serum Albumin (heat shock fraction, $\geq 98\%$ Sigma-Aldrich, USA), distilled water, NaOH crystal pro analyze (Merck KgaA; Darmstadt, Germany), HCl pro analyzes 37%, AgNO_3 , KH_2PO_4 (Merck KgaA; Darmstadt, Germany), sulfanilic acid pro analyzes (Merck KgaA; Darmstadt, Germany), NaNO_2 extra pure for analysis (CIMS, Indonesia), and Na_2CO_3 (Merck KgaA; Darmstadt, Germany).

2.2. Silica extraction and the making of $\text{SiO}_2\text{@BSA}$ adsorbent

The procedure for Silica Extraction from Takari natural sand was obtained from the one carried out by Naat et al. (2018) (20). $\text{SiO}_2\text{@BSA}$ adsorbent was made as follows: 0.2 g of silica was dissolved in 20 mL of phosphate buffer and sonicated for 7 minutes with a power of 50 W. Next, each 10 mL of BSA solution containing 20, 40, 60, 80, and 100 mg/L was prepared separately in phosphate buffer. Then, each BSA solution was interacted with silica suspension, stirred using a magnetic stirrer for 80 minutes, and sonicated for 7 min. The suspension result was centrifuged for 10 minutes at 300 rpm and washed using phosphate buffer and distilled water. Then, the precipitate was filtered and dried at room temperature to produce $\text{SiO}_2\text{@BSA}$ powder (23). Characterization was carried out using FT-IR and SEM.

2.3. Optimization of Tyramine Adsorption

The optimization of the adsorbent mass was carried out at mass variations of 0.02; 0.04; 0.06; 0.08; 0.1; 0.15, and 0.2 g with pH 7. The optimization of pH was carried out with variations of 4; 5; 6; 7, and 8. Temperature optimization was conducted at 30, 40, and 50 °C variations. All treatments were carried out by interacting 25 mL of tyramine solution with $\text{SiO}_2\text{@BSA}$ adsorbent, which was stirred using a magnetic stirrer and, centrifuged for 10 minutes, then filtered. The obtained filtrate was added with Pauly reagent and tested using a UV-Vis spectrophotometer at a wavelength of 470 nm (optimum). The adsorption efficiency represents the tyramine percentage removed during the adsorption process. Mathematically, the tyramine adsorption efficiency can be calculated using the equation (28, 29):

$$\%EP = \frac{(C_0 - C_e)}{C_0} \times 100\% \quad (1)$$

C_0 represents the initial concentration of the solution (mg/L), while C_e represents the residual concentration (mg/L). Adsorption capacity states the amount of adsorbate absorbed in the adsorbent at a specific time (mg/L); mathematically, it can be written as follows (30–32):

$$q_e = \frac{(C_0 - C_e)V}{m} \quad (2)$$

Where V is the volume of the solution (L), and m is the mass of the adsorbent (g).

2.4. Tyramine Adsorption Isotherm Model

25 mL of tyramine solution with various concentrations of 10, 20, 30, 40, and 50 mg/L were put into beakers with pH 5 solution. In each beaker, 0.1 g of $\text{SiO}_2\text{@BSA}$ adsorbent was added. Adsorption was carried out in a batch method for 60 minutes while stirring at a temperature of 303 K. After the adsorption, the solution was centrifuged for 10 minutes. The filtrate was then analyzed using a UV-Vis spectrophotometer at a wavenumber of 470 nm to determine the remaining tyramine concentration (12). The data obtained were used to determine the appropriate adsorption isotherm model for the tyramine adsorption process. The isotherm models used for tyramine adsorption are shown in Table 1.

Table 1: Mathematical model of adsorption isotherm of tyramine using $\text{SiO}_2\text{@BSA}$.

Isotherm Model	Equation	Plotting	Parameter	Reference
Langmuir	$\frac{1}{q_e} = \frac{1}{q_m K_L} \frac{1}{C_e} + \frac{1}{q_m}$	$\frac{1}{C_e}$ vs $\frac{1}{q_e}$	$\frac{1}{q_m}$ = Intercept $q_m = \frac{1}{\text{intercept}}$ $K_L = \frac{1}{q_m \times \text{slope}}$	(26,33)
Freundlich	$\ln q_e = \ln k_f + \frac{1}{n} \ln C_e$	$\ln C_e$ vs $\ln q_e$	$n = \frac{1}{\text{slope}}$ $k_f = e^{\text{intercept}}$	(34)
Temkin	$q_e = B(\ln A) + B(\ln C_e)$	$\ln C_e$ vs q_e	$A = e^{\text{intercept}/B}$ $B = \text{slope}$	(26, 34)
Brunauer-Emmett-Teller (BET)	$\frac{C_e}{[(C_0 - C_e)q_e]} = \frac{1}{B q_m} + \frac{(B-1)C_e}{B q_m C_0}$	$\frac{C_e}{[(C_0 - C_e)q_e]}$ vs $\frac{C_e}{C_0}$	$q_m = \text{intercept}$ $\frac{(B-1)}{q_m} = \text{slope}$	(28)
Redlich-Peterson	$\ln \frac{C_e}{q_e} = \beta \ln C_e - \ln K_R$	$\ln C_e$ vs $\ln \frac{C_e}{q_e}$	$K_R = \text{intercept}$ $\beta = \text{slope}$	(28)
Halsey	$\ln q_e = \frac{1}{n_H} \ln k_H - \frac{1}{n_H} \ln C_e$	$\ln C_e$ vs $\ln q_e$	$n_H = \frac{1}{\text{slope}}$ $k_H = e^{\text{intercept}}$	(26)
Jovanovic	$\ln q_e = \ln q_{\max} - k_J C_e$	C_e vs $\ln q_e$	$q_{\max} = e^{\text{intercept}}$ $k_J = \text{slope}$	(33,36)
Dubinin-Radushkevich	$\ln q_e = \ln Q_s - \beta \epsilon^2$	ϵ^2 vs $\ln q_e$	$\beta = K_{DR} = \text{slope}$ $\ln Q_s = \text{intercept}$	(26)

*Note: The symbol descriptions in Table 1 can be seen in the abbreviations

2.5. Study of Adsorption Thermodynamic of Tyramine

The adsorption thermodynamics was determined by preparing tyramine solutions with 10, 20, 30, 40, and 50 mg/L concentrations at pH 5 of 25 mL each. The solution was then put into vials, and 0.1 grams of $\text{SiO}_2\text{@BSA}$ was added to each vial.

Adsorption was carried out in a batch method while slowly stirring at 303 K for 60 minutes. After the adsorption, each solution was centrifuged at 300 rpm for 10 minutes and filtered. The filtrate was analyzed using a UV-Vis spectrophotometer to determine the residual tyramine concentration. The same procedure was carried out with

temperatures of 313 K and 323 K. For each temperature variation, the respective K values will be obtained. The K value is then plotted between $\ln K$ vs $1/T$, and from this plot, the values of ΔH° and ΔS° can be determined, while ΔG° can be calculated using equation (37):

$$\Delta G^\circ = \Delta H^\circ - T\Delta S^\circ \quad (3)$$

The enthalpy and entropy changes were calculated using Van't Hoff linear equation (37):

$$\ln K_d = \frac{\Delta S^\circ}{R} - \frac{\Delta H^\circ}{RT} \quad (4)$$

K_d represents the equilibrium constant ($K_d = q_e/C_e$), which depends on the tyramine concentration and temperature. R denotes the ideal gas constant ($8.314 \text{ JK}^{-1}\text{mol}^{-1}$), and T represents the absolute temperature (K). The $\ln K_d$ vs. $1/T$ plot data is shown in Figure 6. The value of K_d can be determined from the intercept of the plot of $\ln q_e/C_e$ versus q_e . By plotting $\ln K_d$ versus $1/T$, the values of ΔS° and ΔH° can be determined from the slope and intercept.

3. RESULTS AND DISCUSSION

3.1. Characterization using FT-IR and SEM

SiO_2 and $\text{SiO}_2@\text{BSA}$ characterization using FT-IR showed a stretching vibration of the -OH functional group from the silanol at a wavenumber of

3442.97 cm^{-1} , which decreased in $\text{SiO}_2@\text{BSA}$ to 3294.27 cm^{-1} . A new functional group originating from BSA was shown to be formed at a wavenumber of 2956.13 cm^{-1} , which is the C-H stretching vibration from BSA. In $\text{SiO}_2@\text{BSA}$, there were 2 wave numbers of 1651.61 cm^{-1} and 1535.34 cm^{-1} , respectively, which are the stretching of N-H amide and C-N group on the silica surface due to the adsorption of C-N originating from BSA. The results of FT-IR characterization presented the success of BSA modification seen in the C-H, N-H, and C-N groups which are the typical groups of BSA. This result is consistent with previous research reported by Naat et al. (2021) (37). The results of FT-IR for $\text{SiO}_2@\text{BSA}$ after adsorption showed a stretching vibration originating from the active silica Si-OH group shown on the wave number of 3442.54 cm^{-1} and confirmed by the peak on the adsorption at a wavenumber of 1060.45 cm^{-1} . Asymmetrical bending vibration of the $-\text{NH}_3^+$ group from tyramine at a wavenumber of 1642.54 cm^{-1} underwent an overlap with the stretching vibration of the N-H group from BSA; this result is also in line with the report by Kulik et al. (2010) and Makara et al., (2008) (38, 39). The FT-IR spectra for SiO_2 show peaks at a wavenumber of 1093.27 cm^{-1} and 795.75 cm^{-1} , indicating the asymmetrical and symmetrical stretching vibrations of Si-O in the siloxane (Si-O-Si) structure of SiO_2 . Wavenumbers of 791.05 cm^{-1} and 447.76 cm^{-1} displayed symmetrical stretching vibration from Si-O and the bending vibration from the siloxane group (14, 37, 40).

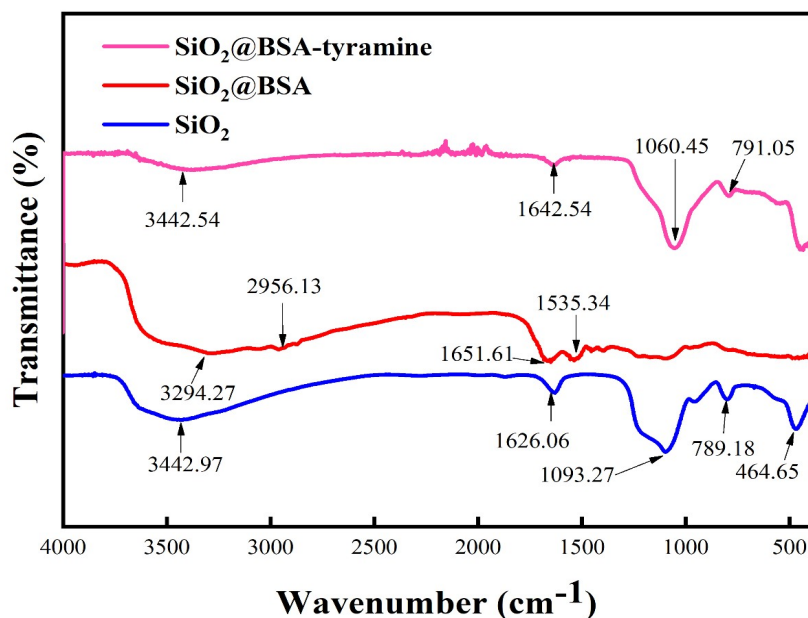


Figure 1: FT-IR spectra of SiO_2 , $\text{SiO}_2@\text{BSA}$, and $\text{SiO}_2@\text{BSA}$ -Tyramine.

Image result of morphology SEM of the $\text{SiO}_2@\text{BSA}$ surface (Figure 2.a) and $\text{SiO}_2@\text{BSA}$ -Tyramine (Figure 2.b) is shown in Figure 2. SEM image of $\text{SiO}_2@\text{BSA}$ before tyramine adsorption showed particles in non-uniform size, unevenly distributed, and agglomerated, creating bigger particles.

$\text{SiO}_2@\text{BSA}$ after tyramine adsorption demonstrated a more apparent difference. The initially clear particle shape turned unseen after adsorption. Surface morphology after adsorption appeared to be more uniformly distributed, with finer shapes and a slightly uneven surface. SEM image showed

that the SiO₂@BSA adsorbent surface had ensnared the tyramine molecule, and the tyramine

molecule itself covered most of the SiO₂@BSA adsorbent surface.

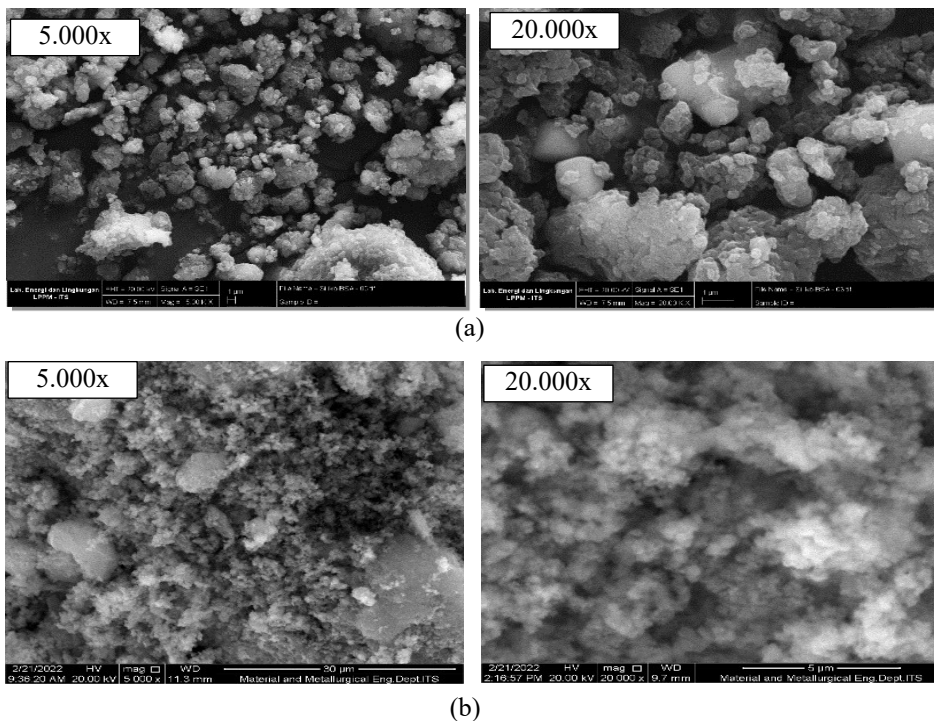


Figure 2: SEM images of SiO₂@BSA specimen (a) before and (b) after tyramine adsorption.

3.2. Optimization of Tyramine adsorption

3.2.1. Optimization of Adsorbent Mass

The result analysis of the tyramine adsorption capacity in each of the SiO₂@BSA adsorbent mass variations is presented in Figure 3.

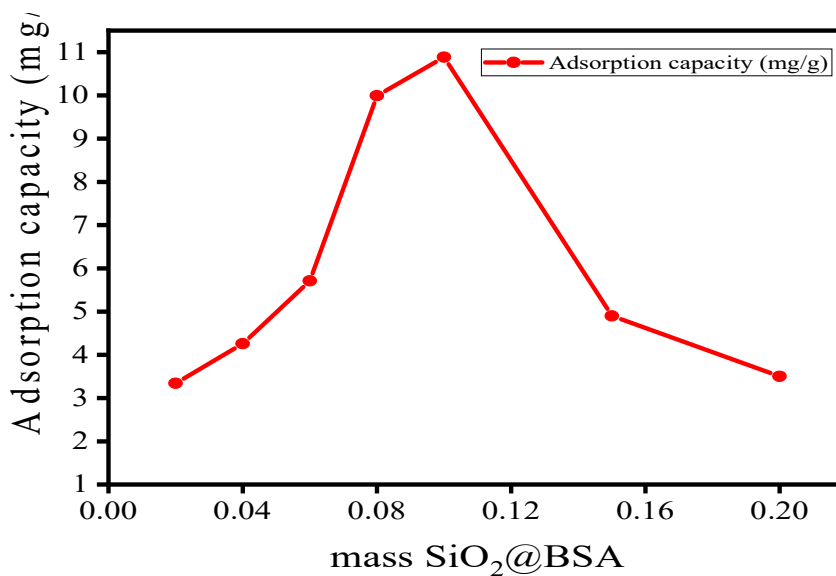


Figure 3: Tyramine adsorption capacity curve according to SiO₂@BSA mass variation.

Figure 3 shows that tyramine adsorption capacity increased to 0.1 grams of SiO₂@BSA mass. This increase resulted from adding an active group (-COOH from BSA) on the SiO₂ surface until reaching the optimum ratio to adsorb tyramine. Meanwhile, there was a regular decrease in tyramine adsorption capacity on 0.15-0.2 grams of SiO₂@BSA mass variation. The decrease in adsorption capacity is due to the BSA polymer overlapping silica surface that further causes interprotein interaction between the electropositive amino group and the electronegative carboxylate

group. The incurred interaction causes the reduction of active adsorbent groups that can interact with tyramine. Therefore, the increased amount of BSA causes the reduced amount of active adsorbent group, thus decreasing tyramine adsorption capacity.

3.2.2. pH Optimization of Tyramine Adsorption

The optimum pH of tyramine adsorption in every pH solution variation of 4-8 is presented in Figure 4.

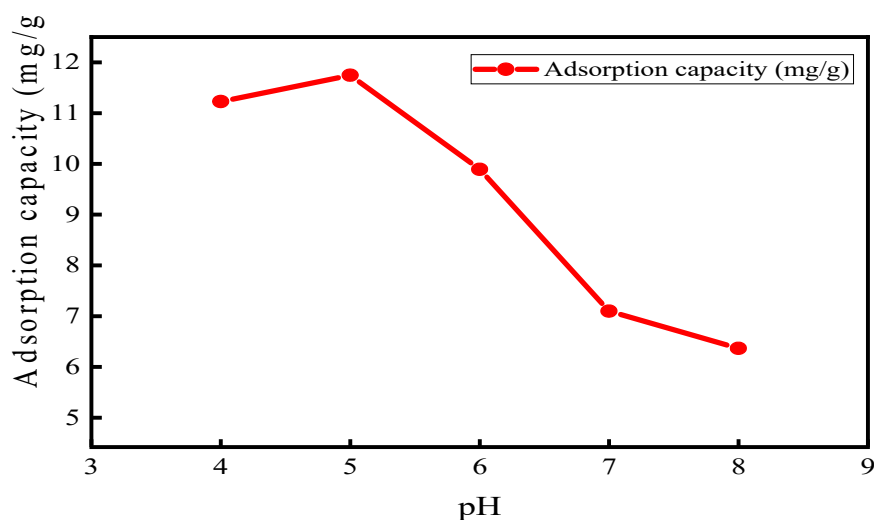


Figure 4: Tyramine adsorption capacity curve according to variation of pH solution.

Figure 4 shows an increased adsorption capacity at pH 4-5. This increase resulted from the hydrogen bond between BSA and tyramine. Adsorption capacity occurred at pH 5 ($q_e=11.74$ mg/g) because BSA tends to be positively charged, which prompts repulsion against tyramine and thus may disrupt the forming of hydrogen bonds between the carboxylate group with tyramine. At pH 5, BSA was in a neutral state; therefore, the forming of hydrogen bonds between BSA and tyramine can proceed well; this is also consistent with a report by Chang et al. (2018) that tyramine bonds with hydrogen through the nitrogen group from amino with oxygen group from the water molecule (41-43). In addition, it is assumed that in this state, there is an H₃O⁺ group that tends to reject tyramine cation and causes the lack of competition between the hydroxide ion of water and the BSA functional group to adsorb tyramine. On the other hand, there was a decrease in adsorption capacity at pH 6 to 8.

Table 2: Data of the Optimization of Tyramine Adsorption using SiO₂@BSA Adsorbent.

Optimized Parameter	Optimum Value	Adsorption Capacity (mg/g)
Adsorbent mass (g)	0.1	10.88
pH	5	11.74
Temperature (K)	303	2.47

Notes: V=25 mL, T=25 °C, C₀ = 50 mg/L, t = 60 min, and stirred with a shaker at 300 rpm

3.3. Tyramine Adsorption Isotherm using SiO₂@BSA adsorbent

Isotherm determination is carried out by varying initial tyramine concentration from 10-50 mg/L. Adsorption efficiency and capacity are calculated using equations 1 and 2, then proceed to make Langmuir, Freundlich, Temkin, Brunauer-Emmett-Teller (BET), Redlich-Peterson, Halsey, and Jovanovic isotherm model graphs as shown in Figure 5.

Table 3: Data of Tyramine Adsorption Isotherm Model Parameter by [SiO₂@BSA](#).

Isotherm Model	Parameter	Value
Langmuir	q_m (mg/g)	5.157
	K_L (L/mg)	1.357
	R^2	0.837
Freundlich	n	3.759
	$K_f K_f$ (L/mg)	2.541
	R^2	0,911
Temkin	B (J/mol)	1.040
	A (L/mg)	11.250
	R^2	0.817
BET	q_m	76.805
	B	24.248
	R^2	0.862
Redlich-Peterson	K_R (L/g)	0.394
	β	0.734
	R^2	0.987
Halsey	n_H	3.759
	k_H	2.541
	R^2	0.911
Jovanovic	Q_{max} (mg/g)	2.601
	k_J (L/mg)	0.042
	R^2	0.888
Dubinin-Radushkevich	$\beta = K_{DR}$	-0.0004
	Q_s	5.381
	R^2	0.755

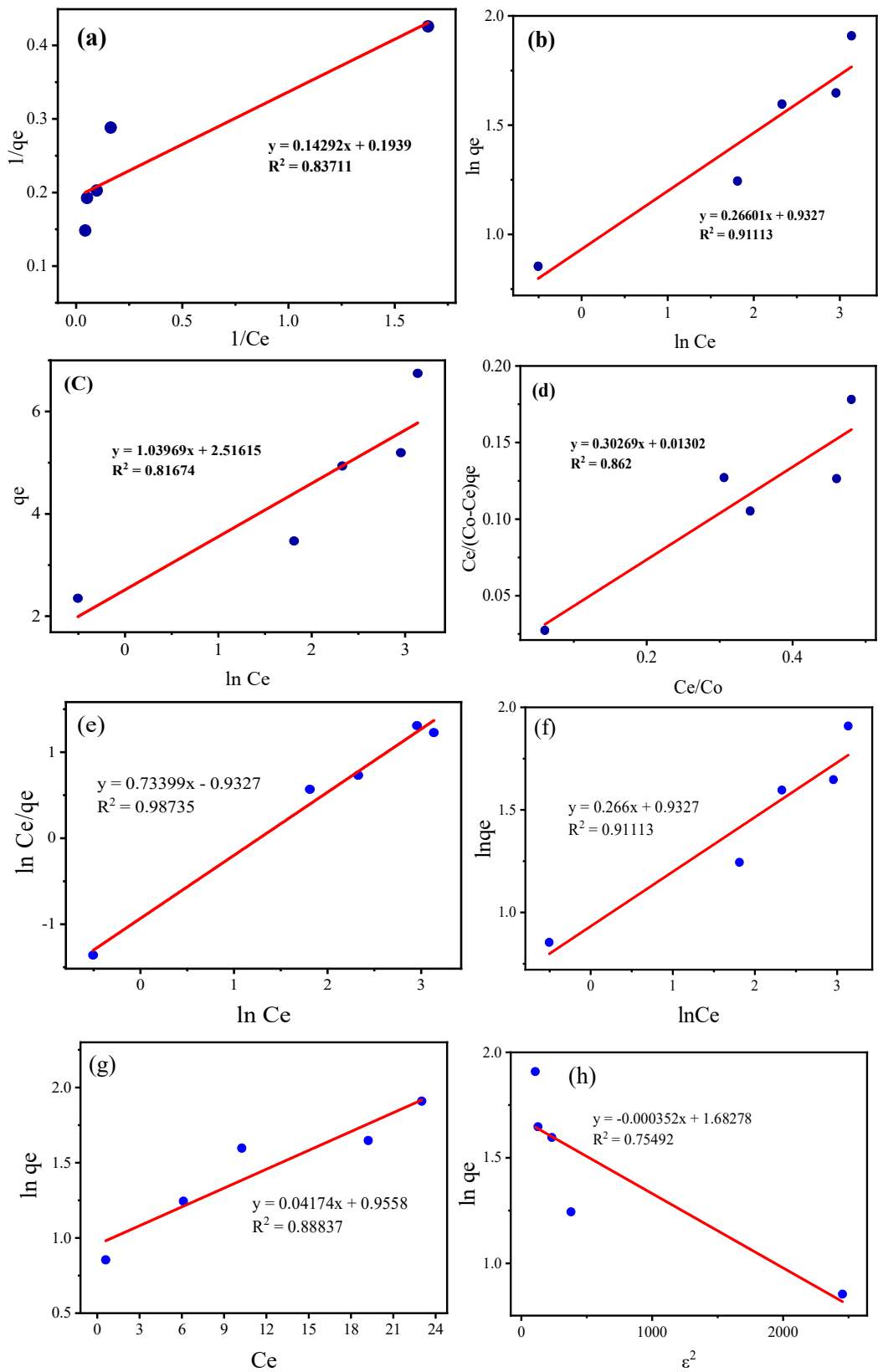


Figure 5: 8 Graphs of tyramine adsorption isotherm model by SiO₂@BSA: (a). Langmuir, (b). Freundlich, (c). Temkin, (d). BET, (e). Redlich-Peterson, (f). Hasley, (g). Jovanovic, (h). Dubinin- Radushkevich.

Figure 5 shows eight isotherm models that have been studied to understand the tyramine adsorption isotherm model using SiO₂@BSA with silica sourced from Takari natural sand. The tyramine adsorption isotherm model by SiO₂@BSA adsorbent adheres to the Redlich-Peterson isotherm model as it possesses a coefficient correlation closer to one ($R^2=0.987$) than another isotherm model. This model is the hybrid model of the Langmuir and Freundlich model that can be applied both in a heterogeneous and homogeneous system. In other words, both models are applicable during this adsorption process (44). This isotherm model shows adsorption equilibrium in a wide range (45). Langmuir isotherm model is referred to in low concentration of tyramine, while

the Freundlich isotherm model in a high concentration of tyramine (44, 46). According to the Langmuir isotherm model, the maximum capacity is at 5.157 mg/g, and the n value in the Freundlich model is obtained as 3.759, which means that the interaction occurred between tyramine and SiO₂@BSA has involved a chemical reaction and formed monolayer coating.

3.4. Adsorption Thermodynamic of Tyramine using SiO₂@BSA

The result analysis of the adsorption thermodynamic of the tyramine parameter by SiO₂@BSA adsorbent is presented in Figure 6 and Table 4.

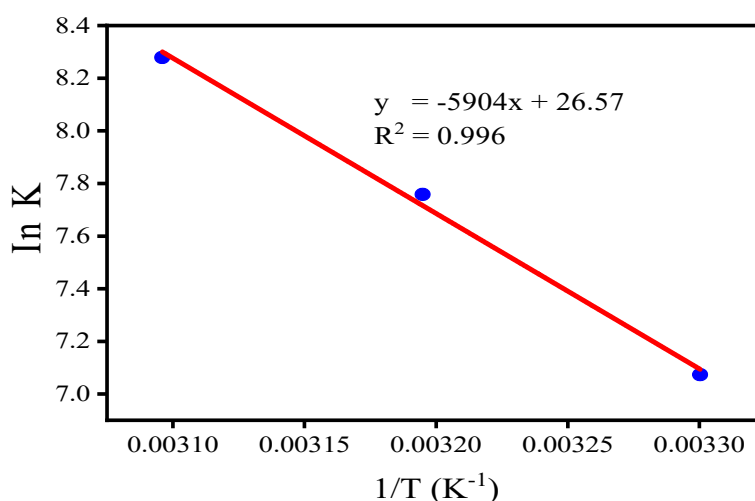


Figure 6: Van't Hoff Adsorption Curve on SiO₂@BSA adsorbent.

Table 4: Thermodynamic parameter values of tyramine adsorption on SiO₂@BSA.

Temperature (K)	ΔG° (kJ/mol)	ΔH° (kJ/mol)	ΔS° (kJ/mol.K)
303	-17.84		
313	-20.05	49.08	0.22
323	-22.26		

Figure 6 and Table 4 indicate that the thermodynamic parameter value presented is ΔH° 49.08 kJ/mol. A positive value shows that the tyramine adsorption process occurred endothermically, which means the reaction absorbed heat and adsorption capacity increased along with the temperature increase (36, 47, 48). From the enthalpy data, it can be stated that the

BSA adsorption process followed a physical-chemical mechanism with a small entropy change ΔS° value of 0.22 kJ/mol which indicates a decrease in randomness or irregularity on the silica surface during the adsorption process. ΔS° value also shows conformity between tyramine adsorbate with the active site of SiO₂@BSA adsorbent and good adsorption reversibility (47-48). The negative Gibbs free energy (ΔG°) values at -17.84; -20.05; -22.26 kJ/mol are at 30, 40, and 50°C, respectively, showing that the adsorption process occurred spontaneously (33). According to the resulting study, it can be concluded that the BSA adsorption process on silica adsorbent occurred endothermically and spontaneously at the temperature of 303 K, and the adsorption occurred as a physical-chemical adsorption type.

Table 5: Comparison of the isotherm and thermodynamic studies of adsorption with several types of SiO₂@BSA and histamine adsorbates.

Adsorbent	Adsorbate	Isotherm models	Thermodynamic (Adsorption Model)	References
Ca-montmorillonite (SAz-2)	Tyramine (TY)	Langmuir	a physical-chemical adsorption type	(14)
Na modified zirconium phosphate Na-ZrP	Tyramine (TY)	Langmuir	-	(18)
SiO ₂ @BSA	Tyramine (TY)	Redlich-Peterson	A physical-chemical adsorption	This study

4. CONCLUSION

Silica extracted from Takari natural sand and modified with BSA has been successfully used to adsorb tyramine. FT-IR and SEM characterization results showed that tyramine adsorbed on the SiO₂@BSA surface. The optimum mass of tyramine adsorption in SiO₂@BSA adsorbent was 0.1 g, with an adsorption capacity of 10.88 mg/g. The optimum pH was at 5 with an adsorption capacity of 11.74 mg/g and an optimum temperature of 303 K with an adsorption power of 2.47 mg/g. Isotherm study showed that adsorption adheres to the Redlich-Peterson isotherm model with an R²=0.987 value with an adsorption capacity equilibrium of 5.157 mg/g and n value of 3.759. The thermodynamic study demonstrated thermodynamic parameter $\Delta H^\circ = 49.08$ kJ/mol, $\Delta G^\circ = -17.84$; -20.05 and -22.26 kJ/mol, also $\Delta S^\circ = 0.22$ kJ/mol.K which showed that tyramine adsorption process on SiO₂@BSA adsorbent occurred endothermically and spontaneously at the temperature of 303 K and the adsorption occurred as a physical-chemical adsorption type.

5. CONFLICT OF INTEREST

The explicit declaration of whether the conflict of interest does or does not exist.

6. ACKNOWLEDGMENTS

The authors are grateful to the "Ministry of Education, Culture, Research, and Technology" for its financial support through the "Cooperation Research between Universities/PKPT" scheme with a master contract number: 041/E5/PG.02.00.PT/2022 and derivative contract number: 55/UN15.19/SP2H/LT/2022.

7. ABBREVIATIONS

q_e : adsorbate concentration at equilibrium time (mg/g); q_t : adsorbate concentration at time t (minutes) (mg/g); k: adsorption rate constant; C_0 : initial concentration of adsorbate in solution (mg/L); C_t : Concentration of tyramine in solution at time t (mg/L); V: volume of solution (mL); EP:

Absorption Efficiency (%); m: adsorbent mass (g); α : (<1); β : desorption constant related to surface area and chemisorption activation energy (mg/g); t: time. q_{max} : the capacity of the adsorbent monolayer (mg/g); K_L : the Langmuir adsorption constant; C_e : the adsorbate equilibrium concentration (mg/L); K_f : Freundlich constant; K_L : the Langmuir adsorption constant; n: the value indicating the degree of linearity between adsorbate solution and the adsorption process; A: the binding equilibrium constant; B: exponent that lies between 0 and 1; K_H dan n: the Halsey model constants; K_J : the Jovanovic constant; B: the Dubinin-Radushkevich isotherm constant; Q_s : refers to the saturation capacity of theoretical isotherms; ϵ : the Polanyi potential (J/mol); K_R : the Redlich-Peterson constants; C_{BET} : Isotherm constant which explains the interaction energy with the surface (L/mg); q_{m-BET} : Isotherm constant which explains theoretical isotherm saturation capacity (mg/g); B_T : the adsorption heat constant; A_T : the binding equilibrium constant; T: the absolute temperature.

8. REFERENCES

1. Finberg JPM & Gillman K. Selective inhibitors of monoamine oxidase type B and the cheese effect. International review of neurobiology. 2011(100):169–190. Available from: <URL>.
2. McCabe-Sellers BJ, Staggs CG & Bogle ML. Tyramine in foods and monoamine oxidase inhibitor drugs: A crossroad where medicine, nutrition, pharmacy, and food industry converge. Journal of Food Composition and Analysis. 2006(19). Available from: <URL>.
3. Halász A, Baráth Á, Simon-Sarkadi L, & Holzapfel W. Biogenic amines and their production by microorganisms in food. Trends Food Sci. Technol. 1994(5):42–49. Available from: <URL>.
4. Santos MHS. Biogenic amines: their importance in foods. 1996 (29):213–231. Available from: <URL>.

5. Andersen G, Marcinek P, Sulzinger N, Schieberle P, and Krautwurst D. Food sources and biomolecular targets of tyramine. *Nutrition reviews*. 2019(77): 107–115. Available from: [<URL>](#).
6. Spano G, Russo P, Lonfau F. Biogenic amines in fermented foods. *Eur J Clin Nutr* 64 (Suppl 3), 2010: S95–S100. Available from: [<URL>](#).
7. Linares DM, del Rio B, Redruello B, Ladero V, Martín MC, Fernández M. Comparative analysis of the in vitro cytotoxicity of the dietary biogenic amines tyramine and histamine. *Food chemistry*, 2016(197):658–663. Available from: [<URL>](#).
8. Loizzo MR, Menichini F, Picci N, Puoci F, Spizzirri UG, Restuccia D. Technological aspects and analytical determination of biogenic amines in cheese. *Trends Food Sci. Technol.*, 2013(30): 38-55. Available from: [<URL>](#).
9. Redruello B, Ladero V, Cuesta I, Álvarez-Buylla JR, Martín MC, Fernández M, Alvarez MA. A fast, reliable, ultra high performance liquid chromatography method for the simultaneous determination of amino acids, biogenic amines and ammonium ions in cheese, using diethyl ethoxymethylenemalonate as a derivatising agent. *Food Chem.* 2013(13): 1029-1035. Available from: [<URL>](#).
10. Jastrzębska, A. A comparative study for determination of biogenic amines in meat samples by capillary isotachopheresis with two electrolyte systems. *Eur Food Res Technol* 2012(235): 563–572. Available from: [<URL>](#).
11. Romano A, Klebanowski H, Guerche SL, Beneduce L, Spano G, Murat ML, Lucas P. Determination of biogenic amines in wine by thin-layer chromatography/densitometry, *Food Chem.* 2012(135): 1392-1396. Available from: [<URL>](#).
12. Vlasova NN, Markitan OV, and Golovkova LP. Adsorption of biogenic amines on albumin-modified silica surface. *Colloid J.* 2011(73): 24–27. Available from: [<URL>](#).
13. Sidorenko IG, Markitan OV, Vlasova NN, Zagorovskii GM, and Lobanov VV. The Adsorption of Biogenic Amines on Carbon Nanotubes. 2009(83): 1139–1142. Available from: [<URL>](#).
14. Chang PH, Jiang WT, and Li Z. Mechanism of tyramine adsorption on Ca-montmorillonite. *Sci. Total Environ.* 2018(642):198–207. Available from: [<URL>](#).
15. Naat J. Pb(II) Adsorption using Silica from Natural Sand of Takari-NTT. *KOVALEN: Jurnal Riset Kimia.* 2022(8): 266-279. Available from: [<URL>](#).
16. Asip F, Mardhiah R, and Husna. Eggshell Effectiveness Test in Adsorbing Fe Ions with Batch Process. *J. Tek. Kim.* 2008(15): 22–26.
17. Suzuki M. [Adsorption Engineering. Tokyo: Kodansha Ltd., 1990.](#)
18. Amghouz Z, Ancín-Azpilicueta C, Burusco KK, García JR, Khainakov SA, Luquin A, Nieto R, & Garrido JJ. Biogenic amines in wine: Individual and competitive adsorption on a modified zirconium phosphate. *Microporous Mesoporous Mater.* 2014(197): 130–139. Available from: [<URL>](#).
19. Buhani and Suharso. Modifikasi silika dengan 3-aminopropiltrimetoksisilan melalui proses sol gel untuk adsorpsi ion Cd(II) dari larutan. *J.Sains MIPA.* 2010(16):177–183.
20. Naat JN, Lapailaka T, Sabarudin A, and Tjahjanto RT. Synthesis And Characterization of Chitosan-Silica Hybrid Adsorbent From The Extraction Of Timor-East Nusa Tenggara Island Silica and its App. *Rasayan J. Chem.* 2018(11):1467–1476.
21. Nurhajawarsi N, Rafi M, Syafitri UD, and Rohaeti E. L-Histidine-Modified Silica from Rice Husk and Optimization of Adsorption Condition for Extractive Concentration of Pb(II). *J. Pure Appl. Chem. Res.* 2018(7):198–208.
22. Alswieleh AM, Modification of Mesoporous Silica Surface by Immobilization of Functional Groups for Controlled Drug Release (2020). Available from: [<URL>](#).
23. Mallakpour S and Nazari HY. The influence of bovine serum albumin-modified silica on the physical-chemical properties of poly(vinyl alcohol) nanocomposites synthesized by ultrasonication technique. *Ultrason. Sonochem.* 2017(41):1–10. Available from: [<URL>](#).
24. Elzoghby AO, Samy WM, and Elgindy NA. Protein-based nanocarriers as promising drug and gene delivery systems. *J. Control. Release.* 2012(161):38–49. Available from: [<URL>](#).
25. Choi JS, and Meghani N. Impact of surface modification in BSA nanoparticles for uptake in cancer cells. *Colloids Surfaces B Biointerfaces.* 2016(145): 653–661. Available from: [<URL>](#).
26. Ragadhita R, Bayu A, and Nandiyanto D. Indonesian Journal of Science & Technology How to Calculate Adsorption Isotherms of Particles Using Two-Parameter Monolayer Adsorption Models and Equations. 2021(6): 205–234. Available from: [<URL>](#).
27. Xu J, Zhen C, Yilin Z, Lou. J. A review of functionalized carbon nanotubes and graphene for heavy metal adsorption from water: Preparation, application, and mechanism. *Chemosphere.* 2018(195):351–364. Available from: [<URL>](#).

28. Naat JN, Neolaka YAB, Lapailaka T, Triandi R, Sabarudin A, Darmokoesoemo H, Kusuma HS. Adsorption of Cu(II) and Pb(II) using Silica@Mercapto(HS@M) hybrid Adsorbent Synthesized from Silica of Takari Sand: Optimization of Parameters and Kinetics, *Rasayan J Chem.* 2021(14):550–560. Available from: [<URL>](#).
29. Aderonke AO, Abimbola BA, Ifeanyi E, Omotayo SA, Oluwagbemiga SA, and Oladotun WM. Adsorption of heavy metal ions onto chitosan grafted cocoa husk char. *African J. Pure Appl. Chem.* 2014(8):147–161. Available from: [<URL>](#).
30. Neolaka YAB, Lawa Y, Naat JN, Riwu AAP, Iqbal M, Darmokoesoemo H, Kusuma HS. The adsorption of Cr(VI) from water samples using graphene oxide-magnetic (GO-Fe₃O₄) synthesized from natural cellulose-based graphite (kusambi wood or *Schleichera oleosa*): Study of kinetics, isotherms and thermodynamics *J. Mater. Res. Technol.* 2020(9):6544–6556. Available from: [<URL>](#).
31. Neolaka YAB, Lawa Y, Naat JN, Riwu AAP, Mango AW, Iqbal M, Darmokoesoemo H, B. Widyaningrum WA, Kusuma HS. Efficiency of activated natural zeolite-based magnetic composite (ANZ-Fe₃O₄) as a novel adsorbent for removal of Cr(VI) from wastewater. *J. Mater. Res. Technol.* 2022(9): 2896–2909. Available from: [<URL>](#).
32. Kali A, Dehmani Y, and Loulidi I. Study of the adsorption properties of an almond shell in the elimination of methylene blue in an aquatic. 2022(3): 509–522. Available from: [<URL>](#).
33. Ayawei N, Ebelegi AN, and Wankasi D. Modelling and Interpretation of Adsorption Isotherms. *J. Chem.* 2017: 1-11. Available from: [<URL>](#).
34. Binaeian E, Mottaghizad M, Hoseinpour AK, and Babae AS. Bovine serum albumin adsorption by Bi-functionalized HMS, nitrilotriacetic acid-amine modified hexagonal mesoporous silicate. *Solid State Sci.* 2020(103): 106194. Available from: [<URL>](#).
35. Al-Ghouti MA and Da'ana DA. Guidelines for the use and interpretation of adsorption isotherm models: A review. *J. Hazard. Mater.* 2020(393):122383. Available from: [<URL>](#).
36. Kouar J, Bellahcen TO, El Amrani A, and Cherif A. Removal of Eriochrome Black T dye from aqueous solutions by using nano- crystalline calcium phosphate tricalcic apatitic. 2021(4):715–727. Available from: [<URL>](#).
37. Naat JN, Neolaka YAB, Lawa Y, Wolu CL, Lestarani D, Sugiarti S, Iswantini D. Modification of Takari natural sand based silica with BSA (SiO₂@BSA) for biogenic amines compound adsorbent. *AIMS Materials Science.* 2022(9): 36-55. Available from: [<URL>](#).
38. Kulik TV, Vlasova NN, Palyanytsya BB, Markitan OV, and Golovkova LP. Spectroscopic study of biogenic amine complexes formed at fumed silica surface. *J. Colloid Interface Sci.* 2010(351): 515–522. Available from: [<URL>](#).
39. Makara K, Misawa K, Miyazaki M, Mitsuda H, Ishiuchi S, and Fujii M. Vibrational Signature of the Conformers in Tyramine Studied by IR Dip and Dispersed Fluorescence Spectroscopies. *J. Phys. Chem.* 2008(112):13463–13469. Available from: [<URL>](#).
40. Timin A, Rummyantsev E, and Solomonov A. Synthesis and application of amino-modified silicas containing albumin as hemoadsorbents for bilirubin adsorption. *J. Non. Cryst. Solids.* 2014(385): 81–88. Available from: [<URL>](#).
41. Yoon I, Seo K, Lee S, Lee Y, and Kim B. Conformational Study of Tyramine and Its Water Clusters by Laser Spectroscopy. *J. Phys. Chem.* 2007(111):1800–1807. Available from: [<URL>](#).
42. Chang P, Jiang W, and Li Z. Mechanism of tyramine adsorption on Ca-montmorillonite. *Sci. Total Environ.* 2018(642):198–207. Available from: [<URL>](#).
43. Malferrari D, Bernini F, Tavanti F, Tuccio L, and Pedone A. Experimental and Molecular Dynamics Investigation Proves That Montmorillonite Traps the Biogenic Amines Histamine and Tyramine. *J. Phys. Chem.* 2017(121). Available from: [<URL>](#).
44. Al-ghouti MA and Da DA. Guidelines for the use and interpretation of adsorption isotherm models: A review. *J. Hazard. Mater.* 2019(393): 122383. Available from: [<URL>](#).
45. Tsai C, Chang W, Saikia D, Wu C, and Kao H. Functionalization of cubic mesoporous silica SBA-16 with carboxylic acid via one-pot synthesis route for effective removal of cationic dyes. Elsevier B.V. 2015: 236-248. Available from: [<URL>](#).
46. Foo KY and Hameed BH. Insights into the modeling of adsorption isotherm systems. *Chem. Eng. J.* 2010(156):2–10. Available from: [<URL>](#).
47. Chaudhry SA, Khan TA, and Ali I. Equilibrium, kinetic and thermodynamic studies of Cr(VI) adsorption from aqueous solution onto manganese oxide coated sand grain (MOCSG). *J. Mol. Liq.,* 2017(236):320–330. Available from: [<URL>](#).
48. Maleki MS, Moradi O, and Tahmasebi S. Adsorption of albumin by gold nanoparticles: Equilibrium and thermodynamics studies. *Arab. J. Chem.* 2015(10):S491–S502. Available from: [<URL>](#).